

ExaFLOW use cases for Nek5000: incompressible jet in cross-flow and flow around a NACA4412 wing section

A. Peplinski¹, R. Vinuesa¹, N. Offermans¹ and P. Schlatter¹

¹*Linné FLOW Centre and Swedish e-Science Research Centre (SeRC), KTH Mechanics
Osquars Backe 18, SE-100 44 Stockholm, Sweden*

1 Introduction

In this document we present simulation setups that will be used within the ExaFLOW project to test Nek5000 in terms of code development. We will consider two main configurations: jet in cross-flow and incompressible flow around a NACA4412 wing section.

The so-called jet in cross-flow (JCF) refers to a configuration in which fluid exits a nozzle and interacts with a boundary layer developing over a flat plate (Figure 1). This case has been extensively studied both experimentally and theoretically over the past decades due to its high practical relevance. It is also considered a canonical flow problem with complex, fully three-dimensional dynamics which makes the JCF a perfect tool for testing numerical methods and simulation capabilities. Recent reviews on this flow configuration are given in Karagozian (2010), Mahesh (2013). Part of this setup is an inflow pipe, which for some tests will be treated separately.

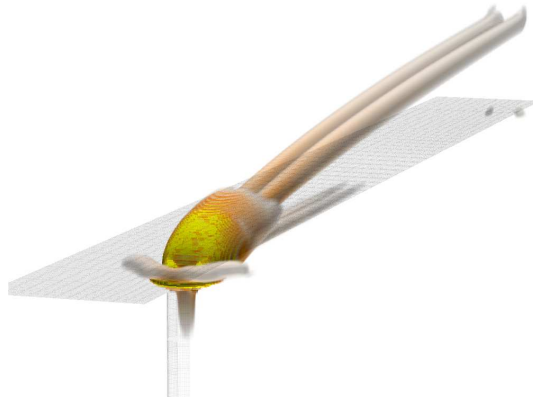


Figure 1: Vortical structures (λ_2 isolevels Jeong & Hussain (1995)) of the base flow for JCF setup including the pipe.

The second configuration under consideration is the incompressible flow around a wing section, represented by a NACA4412 profile. This is an extremely interesting flow case due to the various interacting phenomena present in wings, as observed in Figure 2: laminar-turbulent transition, wall-bounded turbulence under pressure gradients, flow separation and turbulent wake flow. Whereas previous numerical studies of flow around

wings included low-order direct numerical simulations (DNSs) Rodriguez et al. (2013) and large-eddy simulations (LESs) Alferez et al. (2013), as well as high-order DNSs at low Reynolds numbers Shan et al. (2005), we have recently completed a high-order DNS Vinuesa et al. (2015) at an unprecedented Reynolds number of $Re_c = 400,000$ (where Re_c is defined in terms of freestream velocity U_∞ and chord length c). Since a wider scale separation is observed at progressively higher Reynolds numbers, the computing requirements increase dramatically, especially at Reynolds numbers representative of those in academic wind tunnel tests, *i.e.*, from 400,000 up to 1 or 2 million. Hence, this configuration is an excellent test case to evaluate the performance of the various algorithmic developments envisioned in the ExaFLOW project, and to benefit from Exascale capabilities.

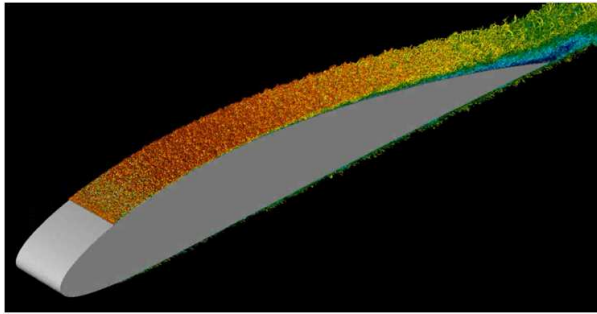


Figure 2: Turbulent structures identified by means of isocontours of the λ_2 criterion Jeong & Hussain (1995) extracted from the NACA4412 wing case.

2 Numerical algorithm

The incompressible Navier-Stokes equations are solved using a spectral element method (SEM) implemented in Nek5000 Fischer, Lottes & Kerkemeier (2008), Fischer & Patera (1994), which is an open-source code developed at the Argonne National Laboratories (Chicago, USA). In SEM the computational domain is decomposed into a set of non-overlapping, high-order, hexahedral sub-domains (elements), where the governing equations are cast into weak form and discretised in space by the Galerkin approximation. C^0 continuity of the variables at the element faces is enforced by direct stiffness summation. Following the $\mathbb{P}_N - \mathbb{P}_{N-2}$ approach the velocity and pressure spaces are locally (within element) spanned by Lagrange polynomial interpolants of order N and $N - 2$ respectively. To ensure flow incompressibility pressure correction scheme is used with the preconditioner based on the additive Schwarz method Fischer (1997). Time integration is based on a generalised BDF k /EXT k scheme. Other discretisation and time integration methods are implemented in Nek5000 as well (*e.g.* $\mathbb{P}_N - \mathbb{P}_N$ and characteristics), however for the ExaFLOW project we will focus on the approach described above.

3 Parallel scaling

Nek5000 is parallelised using the message passing interface (MPI) library. It utilises the natural parallelism of the SEM distributing elements between processors and per-

forming direct stiffness summation in parallel. Parallel performance is improved by use of specialised coarse-grid solvers based on projection scheme (XXT) or algebraic multi-grid (AMG) Fischer, Lottes, Pointer & Siegel (2008). Nek5000 has demonstrated scalability on more than one million ranks, with as few as 5000 grid points per process Fischer, Lottes & Kerkemeier (2008). Results of strong scaling tests of Nek5000 in a number of distributed memory systems are presented in Figure 3.

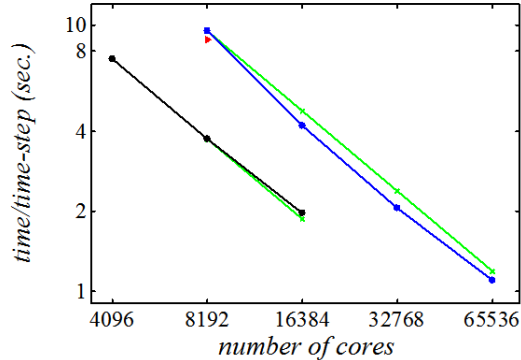


Figure 3: Wall time per time-step for a fixed problem size as a function of number of cores; runs on the systems HECToR (EPCC Edinburgh, UK; \bullet), Triolith (NSC, Sweden; \bullet) and Lindgren (PDC, Sweden; \blacktriangleright). Green line shows the linear scaling. The test case is the turbulent pipe flow described below in Table 1, case 3, with a total of 2.2 billion grid points.

4 Standard input/output

The set of required files to start a simulation consists of `###.rea`, `###.re2`, `###.restart` and `rs8###0.f0000i`, where `###` denotes the corresponding setup name (`jet_crf` for JCF and `naca_wing` for flow around NACA4412 wing section) and $i = 1, 2, 3, 4$. `###.rea` contains the simulation parameters, organised in the following sections:

- real parameters
- passive scalar data
- logical parameters
- mesh description
- restart conditions
- history points
- output specifications

`###.re2` is a binary file containing mesh structure and boundary condition information. The initial condition is stored in the set of files `###.restart` and `rs8###0.f0000i`. A

comprehensive description of configuration files and runtime parameters can be found at http://nek5000.github.io/NekDoc/Nek_users.html.

In the JCF case two additional files are required: `hpts.in` (storing positions of velocity probes) and `###.upar` (containing user-defined parameters). `###.upar` has following structure:

```
&USERPAR      ! probe writing frequency
  UPRMLPRB= 50,
  /
&CHKPOINT     ! checkpoint parameters
  CHKPTSTEP= 50000,
  IFCHKPTRST=F,
  /
```

The simulation output consists of the instantaneous velocity fields saved as `###n.f0000i` (binary files). In the case of the wing, additional binary files with the format `stat000i` are generated, which correspond to turbulence statistics at a number of locations around the wing. In addition to this, it is also possible to use probes to store time histories of various quantities (such as velocity and vorticity components or pressure). The binary files containing the output of the time history series have the format `pts###n.f0000i`.

5 Jet in cross-flow

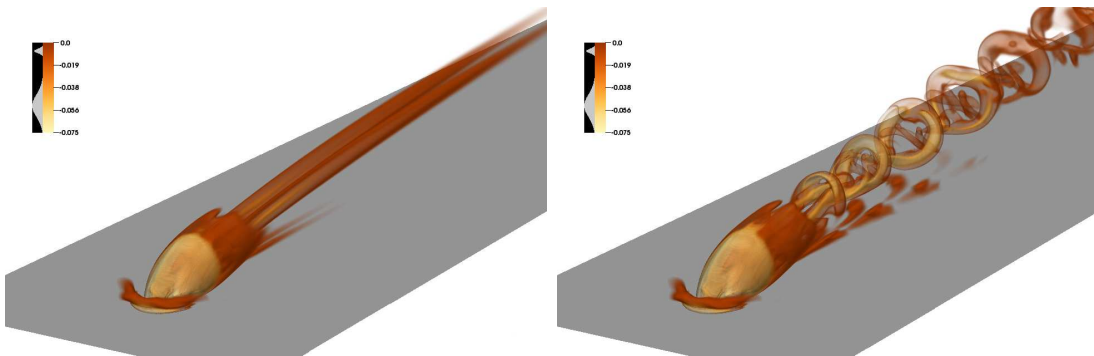


Figure 4: Vortical structures (λ_2 isolevels Jeong & Hussain (1995)) of the JCF for the steady configuration (left) and a periodic vortex shedding (right). Results of the simplified JCF setup without the pipe.

The JCF is characterised by three independent non-dimensional parameters: free-stream Reynolds number ($Re_{\delta_0^*}$), pipe diameter D and jet to free-stream velocity ratio R . As the ratio R increases, the flow evolves from a stable (and thus steady) configuration consisting of (steady) counter-rotating vortex pair (CVP) and horseshoe vortices (left panel in Figure 4), through simple periodic vortex shedding (a limit cycle; right panel in Figure 4) to more complicated quasi-periodic behaviour, before finally becoming turbulent.

In our simulations we consider a circular perpendicular pipe attached to the flat plate (Figure 1) with diameter $D = 3\delta_0^*$, where δ_0^* is the displacement thickness at a position

$7.124\delta_0^*$ upstream from the centre of the pipe orifice (note that δ_0^* is adopted as length unit). The free-stream Reynolds number is $Re_{\delta_0^*} = 200$ and the velocity ratio R is chosen to be close the first bifurcation (between 0.62 and 0.67) making the flow sensitive to the mesh modifications.

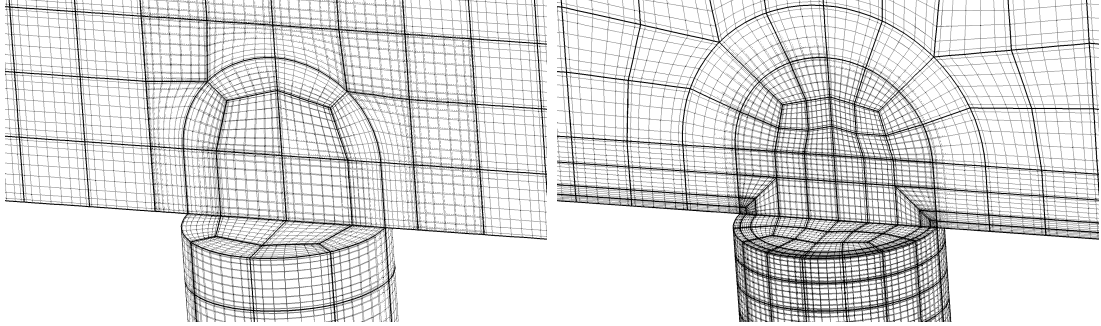


Figure 5: Low (left) and high (right) resolution meshes for JCF. In this Figure we show the mesh structure at the connection between the circular pipe and the rectangular box. The boundaries of the spectral elements are represented by thick lines, whereas the thin ones show the location of the Gauss–Lobatto–Legendre (GLL) points within elements.

The computational domain is composed of a rectangular box and a circular pipe. The mesh structure at the connection between both parts is shown in Figure 5. The size of the rectangular box is set to $L_x = 150$, $L_y = 20$, $L_z = 30$ and is periodic in the spanwise direction. The resolution in this part of the domain is not uniform and we use domain decomposition into elements to reduce the total number of grid points where high resolution is not needed. We keep highest resolution (smallest elements) in the orifice vicinity, and reduce it at larger distances by smooth element stretching. The pipe centre is located 30 units downstream the cross-flow inflow. To investigate the efficiency of adaptive mesh refinement we use number of meshes with different element structure at the pipe inlet but similar resolution at the far field (two examples presented in Figure 5). The lower resolution mesh (left in Figure 5) will be the subject of mesh adaptation, and the high resolution one (right in Figure 5) will provide a reference solution for correctness checks. An additional parameter to control the resolution in the whole domain is the polynomial order N , which will vary from 5 to 11. The total number of grid points will vary between simulations, since the total number of elements and the local polynomial order will be a subject of adaptation.

In our simulations we concentrate on the stability of JCF investigated by linear and non-linear impulse response. In this case we start from evaluation of the steady state for given mesh and parameter set using Selective Frequency Damping. Next we add perturbation to the steady state and measure an amplitude of the strongest mode in the perturbed field. Its time evolution allows us to calculate the mode growth rate, which is a parameter defining linear stability of the system and error measure for our AMR implementation. Figure 6 gives time evolution of the amplitude of the strongest mode for different velocity ratios R with fixed polynomial order $N = 5$ (left panel) and variable N with fixed $R = 0.65$ (right panel). All presented the simulations were performed on low resolution mesh with low amplitude white noise added as perturbation at time $t = 100$. The initial transient growth is clearly visible and is followed by exponential decay (stable

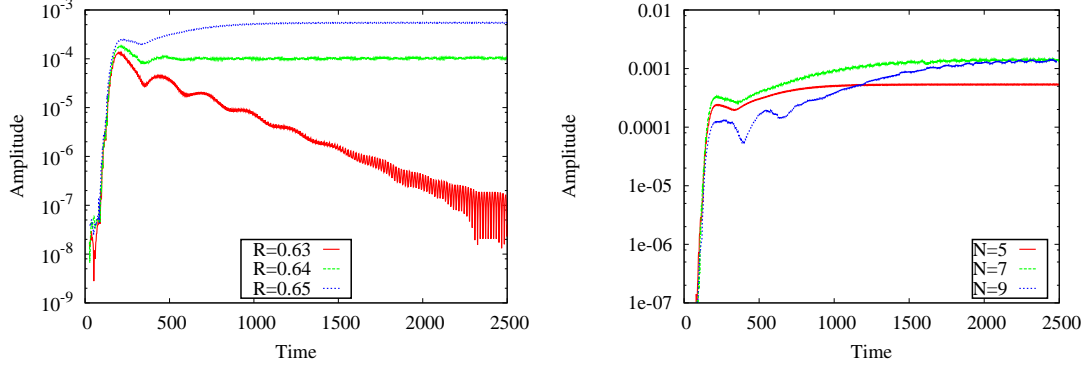


Figure 6: Time evolution of the amplitude of the strongest mode for different velocity ratio R with fixed polynomial order $N = 5$ (left). Right panel shows resolution study for $R = 0.65$ and N ranging from 5 to 9. The transient growth followed by exponential decay/growth phase are clearly visible. For $N = 5$ the bifurcation point is located at $R = 0.64$.

system) or growth (unstable system). Right panel in Figure 6 shows dependency of the growth rate on the mesh resolution, which makes this setup good test case for AMR.

5.1 Turbulent pipe flow

An integral component of the jet in cross-flow configuration, *i.e.*, the turbulent flow through a straight pipe, will be analyzed independently in some of the cases. This is due to the geometrical simplicity of the pipe, which will allow to perform certain tests more easily than in the full JCF setup. A total of three pipe cases are considered, at friction Reynolds numbers Re_τ (based on pipe radius and friction velocity $u_\tau = \sqrt{\tau_w/\rho}$, where τ_w is the wall shear stress and ρ the fluid density) of 180, 550 and 1,000, as summarized in Table 1. The idea is to perform DNSs on the three cases, the first one being aimed at small tests, whereas the remaining two will be used for larger scale runs. Available scaling tests for this configuration can be found in Figure 3. A detailed view of the computational mesh from case 2 is shown in Figure 7, and instantaneous visualizations of the streamwise velocity from cases 2 and 3 can be observed in Figure 8. Note that in all cases a length of $25R$ is considered in the periodic streamwise direction, which is long enough to capture the largest turbulent scales. A complete description of the pipe flow setup can be found in El Khoury et al. (2013).

Case #	Simulation	Re_τ	# grid points
1	DNS	180	19×10^6
2	DNS	550	437×10^6
3	DNS	1,000	2.2×10^9

Table 1: Summary of pipe cases for ExaFLOW project

The strong scaling of the turbulent pipe flow has been performed on several supercomputers for all the Reynolds numbers previously presented. The results for the case $Re_\tau = 550$ on the Cray-XC40 computer “Beskow” at PDC (KTH) are shown in Figure

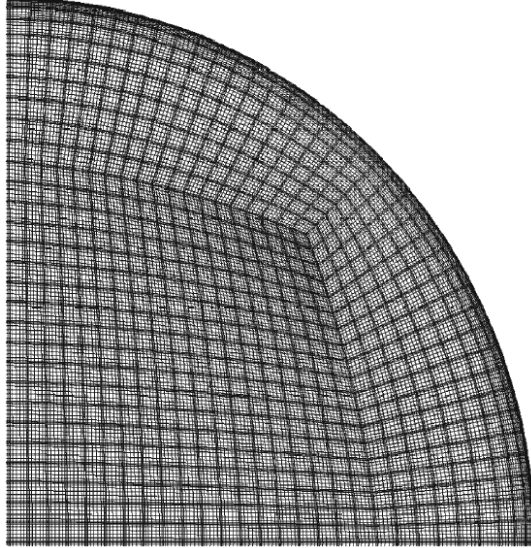


Figure 7: Quarter section of the computational mesh corresponding to case 2 from Table 1, at $Re_\tau = 550$. Spectral element boundaries are shown with thicker lines, whereas thin ones represent the individual GLL points. Polynomial order $N = 7$ was consider in this particular setup.

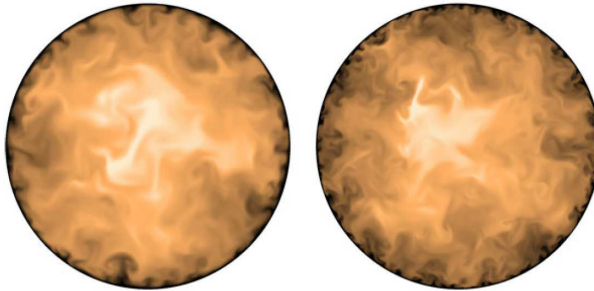


Figure 8: Instantaneous streamwise velocity U normalized with pipe bulk velocity U_b corresponding to cases (left) 2 and (right) 3 from Table 1, at $Re_\tau = 550$ and 1,000 respectively. Note that the velocity varies from 0 (black) to 1.3 (white).

9. The communication, computation and total time for 20 timesteps, excluding I/O, are plotted as a function of the number of nodes. The corresponding number of cores (and MPI ranks) is found by multiplying the number of nodes by 32. The scaling has been performed for both coarse grid solvers XXT and AMG. In general, the difference between XXT and AMG is small but can lead up to a 10% reduction in total time in favor of AMG. We define the strong scaling limit as the point where computation and communication times are equal. On Beskow, it is reached for about 20000 – 50000 gridpoints per core.

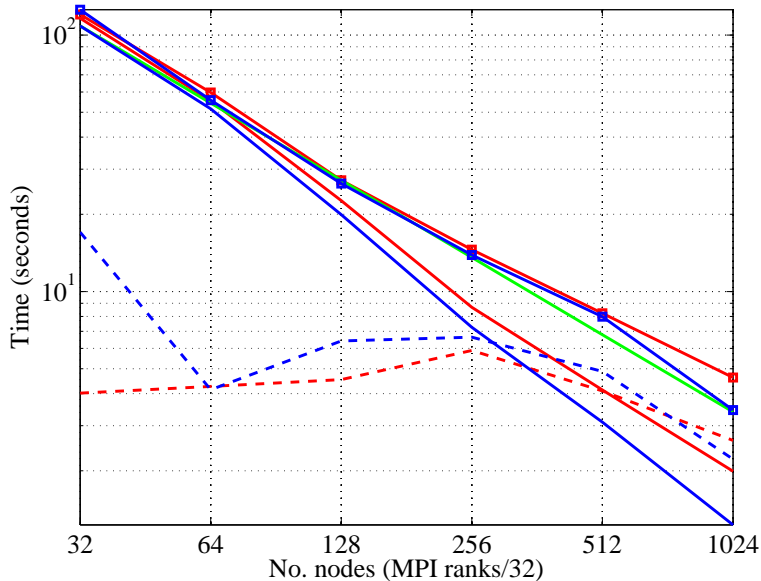


Figure 9: Strong scaling of the turbulent flow in a pipe for $Re_\tau = 550$ on Beskow. AMG (blue), XXT (red), communication (dashed), computation (solid), total time (\square), computational linear scaling (green).

6 Incompressible flow around a NACA4412 wing section

We will consider a total of 5 test cases based on the incompressible turbulent flow around a NACA4412 wing section, at Reynolds numbers Re_c ranging from 50,000 to 1,000,000, all of them with 5° angle of attack. The airfoil geometry includes a sharp trailing edge, obtained by modifying the corresponding coefficient in the NACA airfoil equation. Initially a RANS simulation is performed by means of the code EDGE developed at FOI Eliasson (2002), which uses the explicit algebraic Reynolds stress model (EARSM) by Wallin and Johansson Wallin & Johansson (2000). The RANS domain extends up to $200c$ in every direction, and this RANS solution is used to extract an accurate velocity distribution in the near field corresponding to the time-averaged flow at a given angle of attack. This distribution is then imposed as Dirichlet boundary conditions on the DNS domain. We considered a C-mesh topology of radius c centered at the leading edge of the airfoil, with total domain lengths of $6.2c$ in the horizontal (x), $2c$ in the vertical (y) and $0.1c$ in the spanwise (z) directions, see Figure 10. Periodicity is imposed in the spanwise direction, and the natural stress-free boundary condition at the outlet. The computational mesh was optimized based on distributions of the Kolmogorov scale $\eta = (\nu^3/\varepsilon)^{1/4}$, where ν is the kinematic viscosity and ε is the local isotropic dissipation. The design criterion was $h \equiv (\Delta x \cdot \Delta y \cdot \Delta z)^{1/3} < 4 - 5\eta$ everywhere in the domain, which ensures that the mesh is fine enough to capture the smallest turbulent scales. Note that the flow is tripped at $x/c = 0.1$ on both suction and pressure sides, using the volume forcing approach by Schlatter and Örlü Schlatter & Örlü (2012). The initial condition is the RANS solution, and the flow is initially run for around three flow-over times with polynomial order $N = 5$.

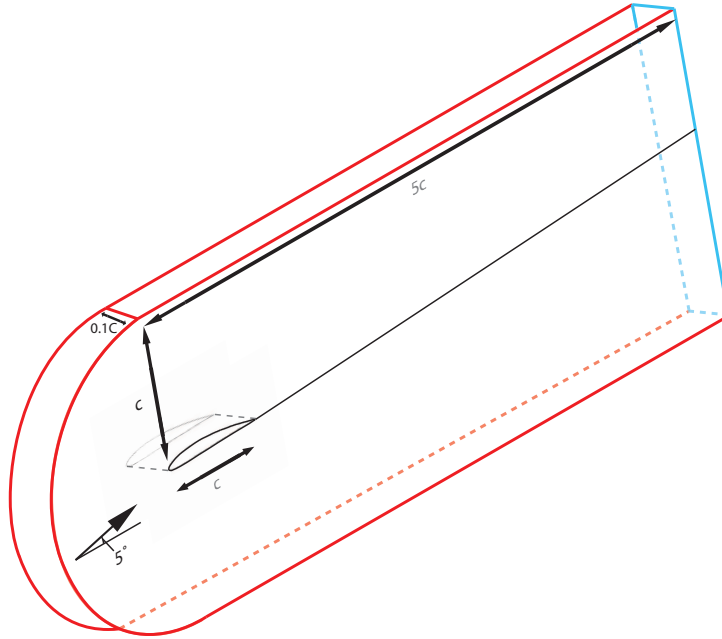


Figure 10: Schematic three-dimensional layout of the set up for direct numerical simulation. The chord length is denoted as c . The domain extends to up $5c$ downstream, and $1c$ upstream, top and bottom from the leading edge. The red lines mark the boundaries where the Dirichlet condition was used. The blue line indicates the boundaries with the stress-free condition. The incoming flow has an angle of attack of 5° , and the Cartesian coordinate system is aligned with the chord.

After this point the polynomial order is progressively increased up to the final value of $N = 11$. A full description of the setup is given by Vinuesa *et al.* Vinuesa et al. (2015) for a case with $Re_c = 400,000$, where 1.85 million spectral elements with $N = 11$ were used, which leads to a total of 3.2 billion grid points. An instantaneous visualization of the flow field, together with the spectral element mesh from the $Re_c = 400,000$ case, are shown in Figure 12. The smoothness of even the smallest vortical structures shows that the setup is appropriate to simulate all the relevant flow features.

The wing cases under consideration for the ExaFLOW project are summarized in Table 2, including a 2D simulation at low Reynolds number, and both direct numerical and large-eddy simulation cases, in order to cover a wide range of scaling effects. Note that the LES is based on the approach proposed by Schlatter *et al.* Schlatter et al. (2004), where a dissipative relaxation term is added to the right-hand side of the Navier–Stokes equations. This term provides all the necessary drain of energy out of the coarsely discretized system, and previous validations in zero pressure gradient boundary layers Eitel-Amor et al. (2014) show excellent agreement between DNS and LES.

Scaling tests performed at the Cray-XC40 computer “Beskow” at PDC (KTH) are shown in Figure 11, for case 3 from Table 2 (left) and for a configuration similar to case 2 with a total of 120 million grid points (right). In order to establish a good measure of scaling, we report the time required to perform one GMRES (generalized minimal residual method) iteration for the pressure solve. Doing so, we can characterize code performance by isolating it from other factors contributing to the total time per time-step, such as I/O

Case #	Simulation	Re_c	# grid points
1	2D	50,000	88×10^3
2	DNS	100,000	82×10^6
3	DNS	400,000	3.2×10^9
4	LES	400,000	530×10^6
5	LES	1,000,000	6.0×10^9

Table 2: Summary of wing cases for ExaFLOW project

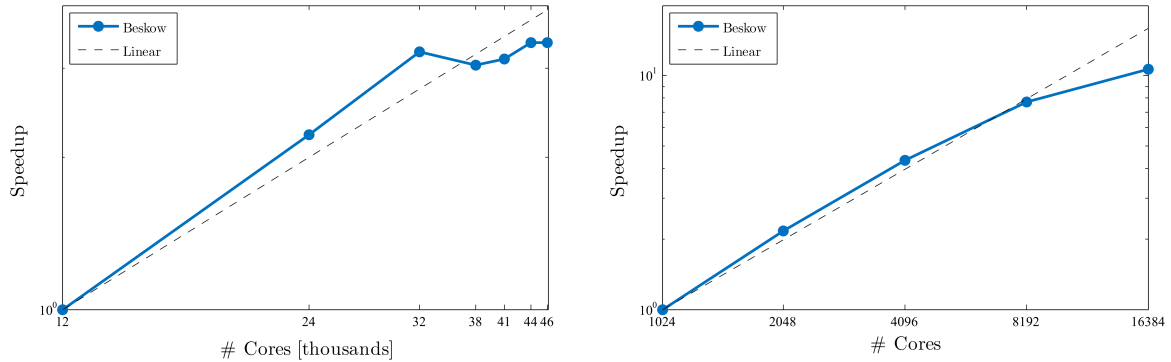


Figure 11: Strong scaling results performed on the “Beskow” system at PDC (KTH). Test cases with a total of (left) 3.2 billion and (right) 120 million grid points.

operations, different tolerances etc. Note that in case 3 the best performance is achieved when running on 32,768 cores (with around 100,000 grid points per core), and in the modified case 2 the best scaling is observed on 4,096 cores, with a total of 30,000 grid points per core.

References

- Alferez, N., Mary, I. & Lamballais, E. (2013), ‘Study of stall development around an airfoil by means of high fidelity large eddy simulation’, *Flow Turbulence Combust* **91**(3), 623–641.
URL: <http://dx.doi.org/10.1007/s10494-013-9483-7>
- Eitel-Amor, G., Örlü, R. & Schlatter, P. (2014), ‘Simulation and validation of a spatially evolving turbulent boundary layer up to $re\theta = 8300$ ’, *International Journal of Heat and Fluid Flow* **47**, 57–69.
- El Khoury, G. K., Schlatter, P., Noorani, A., Fischer, P. F., Brethouwer, G. & Johansson, A. V. (2013), ‘Direct numerical simulation of turbulent pipe flow at moderately high reynolds numbers’, *Flow, turbulence and combustion* **91**(3), 475–495.
- Eliasson, P. (2002), Edge, a navier-stokes solver for unstructured grids., *in* D. Kroner & R. Herbin, eds, ‘Proceedings to Finite Volumes for Complex Applications III.’, Hemre Penton Science London, pp. 527–534.

- Fischer, P. F. (1997), ‘An Overlapping Schwarz Method for Spectral Element Solution of the Incompressible Navier Stokes Equations’, *Journal of Computational Physics* **133**, 84–101.
- Fischer, P. F., Lottes, J. W. & Kerkemeier, S. G. (2008), ‘nek5000 Web page’. <http://nek5000.mcs.anl.gov>.
- Fischer, P. F. & Patera, A. T. (1994), ‘Parallel simulation of viscous incompressible flows’, *Annual Review of Fluid Mechanics* **26**, 483–527.
- Fischer, P., Lottes, J., Pointer, D. & Siegel, A. (2008), ‘Petascale algorithms for reactor hydrodynamics’, *Journal of Physics Conference Series* **125**(1), 012076.
- Jeong, J. & Hussain, F. (1995), ‘On the identification of a vortex’, *Journal of Fluid Mechanics* **285**, 69–94.
- Karagozian, A. R. (2010), ‘Transverse jets and their control’, *Progress in Energy and Combustion Science* **36**, 531–553.
- Mahesh, K. (2013), ‘The interaction of jets with crossflow’, *Annual Review of Fluid Mechanics* **45**, 379–407.
- Rodríguez, I., Lehmkuhl, O., Borrell, R. & Oliva, A. (2013), ‘Direct numerical simulation of a {NACA0012} in full stall’, *International Journal of Heat and Fluid Flow* **43**, 194 – 203. 7th International Symposium on Turbulence Heat & Mass Transfer (THMT-7), PalermoConference on Modelling Fluid Flow (CMFF12).
URL: <http://www.sciencedirect.com/science/article/pii/S0142727X13000891>
- Schlatter, P. & Örlü, R. (2012), ‘Turbulent boundary layers at moderate reynolds numbers: inflow length and tripping effects’, *Journal of Fluid Mechanics* **710**, 5–34.
- Schlatter, P., Stolz, S. & Kleiser, L. (2004), ‘Les of transitional flows using the approximate deconvolution model’, *International journal of heat and fluid flow* **25**(3), 549–558.
- Shan, H., Jiang, L. & Liu, C. (2005), ‘Direct numerical simulation of flow separation around a {NACA} 0012 airfoil’, *Computers & Fluids* **34**(9), 1096 – 1114.
URL: <http://www.sciencedirect.com/science/article/pii/S0045793004001203>
- Vinuesa, R., Hosseini, S. M., Hanifi, A., Henningson, D. S. & Schlatter, P. (2015), ‘Direct numerical simulation of the flow around a wing section using high-order parallel spectral methods’, *Int. Symp. Turbulence & Shear Flow Phenomena (TSFP-9)* **30**.
- Wallin, S. & Johansson, A. V. (2000), ‘An explicit algebraic reynolds stress model for incompressible and compressible turbulent flows’, *Journal of Fluid Mechanics* **403**, 89–132.

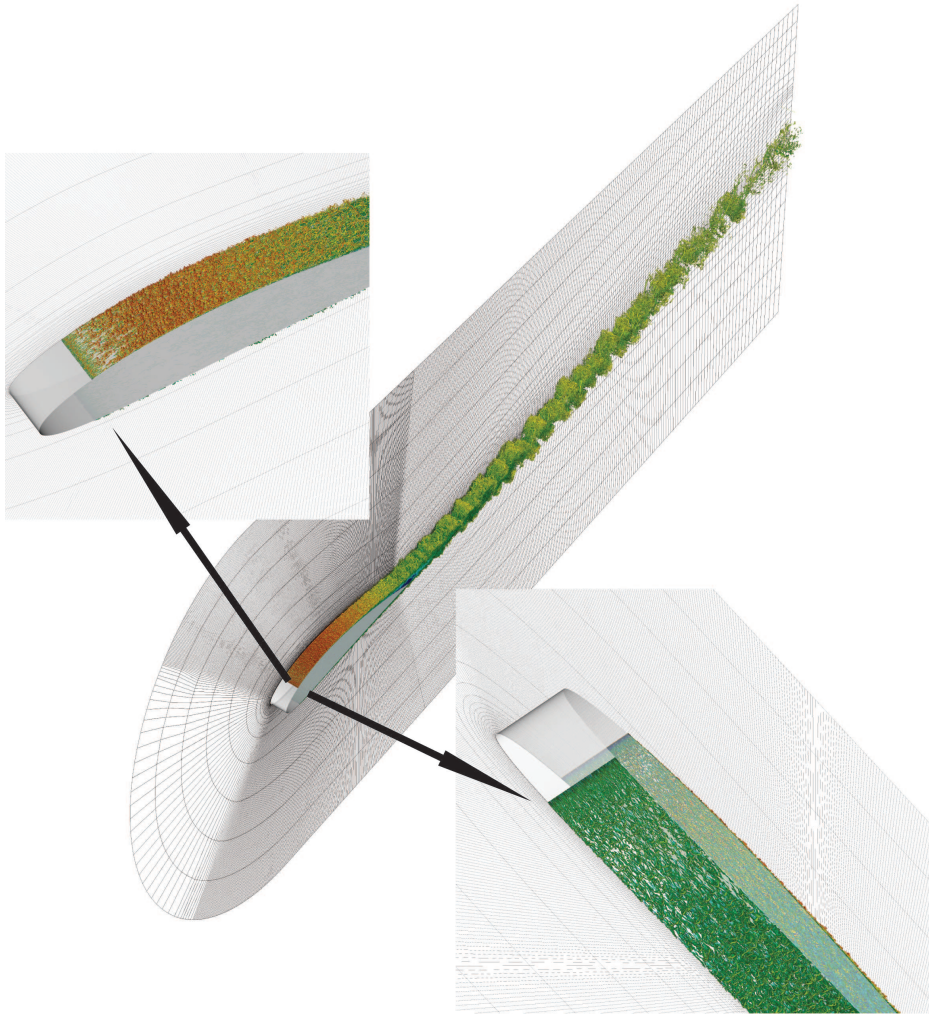


Figure 12: Instantaneous vortical structures visualized with the λ_2 criterion Jeong & Hussain (1995), colored with chordwise velocity, ranging from -0.1 (dark blue) to 1.5 (red). The flow is tripped at 10% chord on both sides. The angle of attack is 5° and the chord Reynolds number is $Re_c = 400,000$. The spectral element mesh is also shown, but not the individual grid points within elements.